



Photoresponsivity enhancement in monolayer MoS₂ by rapid O₂:Ar plasma treatment

Cite as: Appl. Phys. Lett. **114**, 091103 (2019); <https://doi.org/10.1063/1.5086726>

Submitted: 22 December 2018 . Accepted: 16 February 2019 . Published Online: 04 March 2019

Jakub Jadwiszczak , Gen Li, Conor P. Cullen, Jing Jing Wang, Pierce Maguire, Georg S. Duesberg, James G. Lunney, and Hongzhou Zhang 



View Online



Export Citation



CrossMark

ARTICLES YOU MAY BE INTERESTED IN

[Silicon photonic crystal cavities at near band-edge wavelengths](#)

Applied Physics Letters **114**, 091101 (2019); <https://doi.org/10.1063/1.5067358>

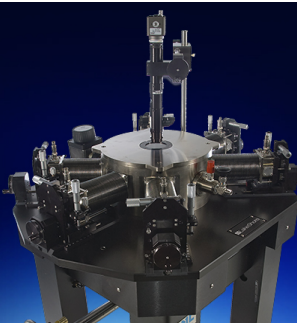
[The discrete noise of magnons](#)

Applied Physics Letters **114**, 090601 (2019); <https://doi.org/10.1063/1.5088651>

[A critical review of recent progress on negative capacitance field-effect transistors](#)

Applied Physics Letters **114**, 090401 (2019); <https://doi.org/10.1063/1.5092684>

 Lake Shore
CRYOTRONICS



Cryogenic probe stations

for accurate, repeatable
material measurements

LEARN MORE 

AIP
Publishing

Photoresponsivity enhancement in monolayer MoS₂ by rapid O₂:Ar plasma treatment

Cite as: Appl. Phys. Lett. **114**, 091103 (2019); doi: [10.1063/1.5086726](https://doi.org/10.1063/1.5086726)

Submitted: 22 December 2018 · Accepted: 16 February 2019 ·

Published Online: 4 March 2019



View Online



Export Citation



CrossMark

Jakub Jadwiszczak,^{1,2} Gen Li,^{1,2} Conor P. Cullen,^{2,3} Jing Jing Wang,² Pierce Maguire,^{1,2} Georg S. Duesberg,^{2,3,4} James G. Lunney,¹ and Hongzhou Zhang^{1,2,a)}

AFFILIATIONS

¹School of Physics, Trinity College Dublin, Dublin 2, Ireland

²Centre for Research on Adaptive Nanostructures and Nanodevices (CRANN) and Advanced Materials and Bioengineering Research (AMBER) Research Centers, Trinity College Dublin, Dublin 2, Ireland

³School of Chemistry, Trinity College Dublin, Dublin 2, Ireland

⁴Institute of Physics, EIT 2, Faculty of Electrical Engineering and Information Technology, Universität der Bundeswehr München, Werner-Heisenberg-Weg 39, 85577 Neubiberg, Germany

a) honzhang@tcd.ie

ABSTRACT

We report up to ten-fold enhancement of the photoresponsivity of monolayer molybdenum disulfide (MoS₂) by treatment with O₂:Ar (1:3) plasma. We characterize the surface of plasma-exposed MoS₂ by TEM, Raman, and PL mapping and discuss the role of MoO_x in improving the photocurrent generation in our devices. At the highest tested laser power of 0.1 mW, we find ten-fold enhancements to both the output current and carrier field-effect mobility at the illumination wavelength of 488 nm. We suggest that the improvement of electrical performance is due to the surface presence of MoO_x resulting from the chemical conversion of MoS₂ by the oxygen-containing plasma. Our results highlight the beneficial role of plasma treatment as a fast and convenient way of improving the properties of synthetic 2D MoS₂ devices for future consideration in optoelectronics research.

Published under license by AIP Publishing. <https://doi.org/10.1063/1.5086726>

Two-dimensional layered transition metal dichalcogenides (TMDs) have attracted wide research interest due to their intriguing physical properties and potential applications. Molybdenum disulfide (MoS₂), a typical layered TMD, is a semiconductor with a direct bandgap of ~1.8 eV in the single-layer limit.¹ This allows monolayer MoS₂ field-effect transistors (FETs) to achieve high ON/OFF ratios² (10⁷–10⁹), making them attractive candidates for switching components in future electronics. Recently, optoelectronic devices fabricated from MoS₂ have received notable attention.^{3,4} MoS₂ phototransistors are easy to fabricate, respond to a wide range of wavelengths,^{3,5} and exhibit fast DC photoresponses.^{6,7} In addition, their photoresponsivity can be tuned by various methods, such as back-gating,^{8,9} strain engineering,¹⁰ layer decoupling,¹¹ and evaporation of sub-stoichiometric molybdenum oxide overlayers.¹² Surface sensitization of monolayer MoS₂ FETs has also yielded significant enhancements of the measured photocurrent in the case of quantum dots,^{13–15} organic molecules,^{16–18} and metal nanostructures.^{19,20} However, these methods often involve additional preparation steps in order to fabricate the sensitizing species and deposit it on the MoS₂ device. Moreover, the surface-deposited

dopants may not be robust to mechanical stressing or further material modification without losing their favorable properties.

Plasma functionalization, in turn, presents a fast and facile way to alter the crystal structure of on-chip layered materials such as MoS₂. It facilitates large-scale, multi-sample, and rapid tuning of the optoelectronic performance of FETs based on layered semiconductors. In particular, oxygen-containing plasmas tend to form sub-stoichiometric molybdenum oxides on the surface of MoS₂.^{21–23} These oxide centres can then act as dopants that alter the charge concentration in the modified MoS₂ transistor channel,^{24–26} and ultimately govern the electron conduction behavior of the newly formed oxide/MoS₂ heterostructure.²⁷ In this work, we demonstrate the enhancement of the photoresponsivity of chemical vapour deposition (CVD)-grown monolayer MoS₂ by O₂:Ar (1:3) plasma treatment. The photoresponsivity is improved ten-fold in gated devices after 2 s of exposure to the plasma. At the same time, the field-effect mobility of the device under illumination improves by over one order of magnitude. We carry out transmission electron microscopy (TEM) imaging and spectroscopic mapping to characterize the sample after plasma exposure and

attribute the observed photoresponse to the suppressed charge recombination mediated by surface-bound molybdenum oxides.

MoS₂ samples were synthesized on SiO₂/Si substrates using the CVD method previously reported.²⁸ The flake thickness was confirmed by optical microscopy and Raman spectroscopy. Standard EBL was carried out to fabricate the FET devices using PMMA resist and development in methyl isobutyl ketone:isopropyl alcohol (MIBK: IPA) (1:3). This was followed by metallization with Ti(10 nm)/Au(40 nm) contacts and lift-off in acetone. Plasma treatment was carried out on a Fischione Instruments 1020 cleaner for 2 s, utilizing O₂:Ar (1:3) gas at a pressure of ~5 mbar. The electrical testing was performed at room temperature in a two-probe configuration (Imina miBot) using a source meter unit (Agilent B2912A) in the ambient. The devices were back-gated through the heavily p-doped Si substrate underneath the 285 nm SiO₂ overlayer. A 488 nm laser was used for irradiation. Its power density was tuned at five different levels and controlled to ensure no fluctuation throughout the experiment. The laser was directed through a condenser lens (20×, NA = 0.4), and the spot size was 1.5 μm. TEM was carried out on a FEI Titan 80–300 system operating at 300 kV. Monolayer samples were transferred onto copper grids using a polymer stamp. Fabricated devices were imaged using a Zeiss Nanofab helium ion microscope at a beam energy of 25 keV. Raman and photoluminescence (PL) spectra were acquired using a WITec Alpha 300R system (λ = 532 nm). A low laser power (<100 μW) was used during mapping to minimize any laser-induced damage or heating of the sample.

The inset of Fig. 1(a) is a false-color helium ion micrograph of a typical contacted device. The contacts in our devices were always deposited in a parallel geometry, as visible in the image. The transistor channel length was over 5 μm to confine the laser irradiation solely to the MoS₂ region. We collected the output and transfer characteristics of the device under 5 different illumination powers. As the laser spot avoided the Au electrodes during illumination, we assume that all of the measured photo-generated current originated from the MoS₂ semiconductor.

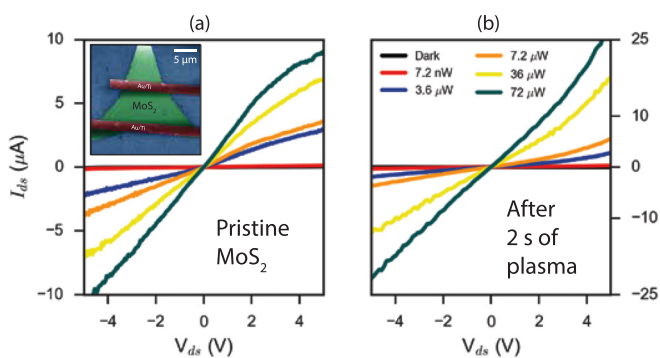


FIG. 1. (a) Output curves of the untreated device, demonstrating a good ohmic contact between the material and the metal electrode. The output current, I_{ds} , increases with increasing laser power under illumination. Inset: false-color helium ion micrograph of a typical contacted monolayer MoS₂ phototransistor device. The blue area is the SiO₂ substrate. (b) Post-plasma treatment IV curves show a similar trend with increasing laser power. The generated photocurrent at high laser powers has increased by up to 3 times at the same applied voltage after 2 s of plasma exposure. We note that no gate bias was applied. The color legend applies to both (a) and (b).

Figure 1(a) shows the output characteristics of the device under laser illumination before any plasma treatment. Prior to any exposure to the plasma, the low-bias IV response of the MoS₂ FET shows a well-behaved linear increase with applied bias for both voltage polarities, indicating good ohmic contacts to the semiconductor. Upon successive irradiations with rising laser power, the photocurrent increases, which is typical for semiconducting monolayer MoS₂ devices.^{3,6,8,29–31} The output current reaches nearly 10 μA at ±5 V at the highest tested laser power of 72 μW. Figure 1(b) tracks the IV curves after 2 s of exposure to the plasma. We see that the current increases to nearly 25 μA at the highest illumination power, compared with the untreated sample at the same applied drain-source voltage. This indicates that dopants introduced by the plasma treatment to the MoS₂ surface mediate an enhanced charge carrier photo-generation response in the device. We note that longer plasma treatments (>2 s) lead to a significant decay of electrical performance and do not enhance the photoresponsivity (see Fig. S2).

Figure 2(a) shows the transfer curves for the same sample before any plasma treatment. Our as-grown devices perform as standard n-type FETs with a field-effect mobility (μ) of 0.13 cm² V⁻¹ s⁻¹ under no illumination, extracted in the linear region of the transfer curve and at $V_{ds} = 1$ V. Upon successive laser irradiations, we observe a photogating effect, whereby the threshold voltage of the transistor shifts to negative gate biases by more than 10 V due to increased electron doping. This has previously been observed in ultrathin TMD FETs and is

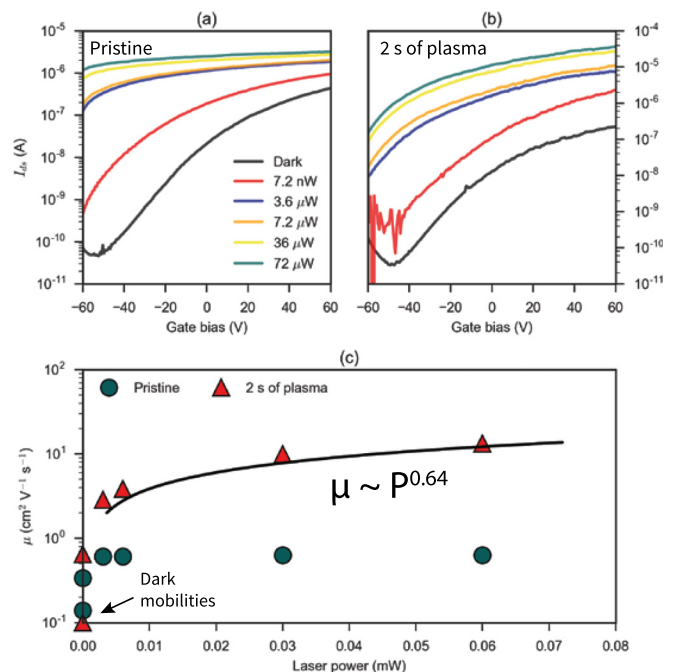


FIG. 2. (a) Transfer characteristics of the untreated device, demonstrating the standard n-type FET behaviour and increase in carriers in the channel at higher laser powers. (b) In the post-treatment gate curves, the level of current has increased by one order of magnitude at all illumination laser powers. The color legend applies to both (a) and (b). (c) Mobility comparison before and after plasma treatment as a function of laser power. The solid black line is a fit to the mobility scaling of the treated sample above 10⁻³ mW.

attributed to the interaction of photo-generated carriers with charge traps in the transistor channel.^{32,33} At the highest incident power, the FET channel is effectively still open at $V_g = 60$ V, where the output current stays firmly above 10^{-7} A and leads to a large reduction in the ON/OFF ratio of our device.

Figure 2(b) presents the gate curves after plasma treatment. The observed level of output current in the dark transfer curve drops two-fold when evaluated at the gate bias, $V_g = 60$ V. Meanwhile, the threshold voltage is seen to shift to more positive gate biases by ~ 5 V. This shift indicates oxygen-related p-type doping in the material, consistent with previous works on oxygen plasma-treated MoS₂.^{21,22,26,34} In addition, the MoS₂ now possesses a weak ambipolar response, indicating hole-branch conduction caused by the likely presence of plasma-created oxides.^{35,36} After 2 s of plasma treatment, the output current in the saturation region of the gate curve improves by one order of magnitude under all illumination powers (note scale on the y-axis). Figure 2(c) tracks the MoS₂ channel field-effect mobility before and after chemical reaction with the plasma. With no laser illumination, the mobility is seen to decrease slightly after 2 s, which we have explored in previous work.²⁵ After 2 s of exposure, the carrier mobility increases over ten-fold in illuminated gate curves, as the laser power is turned up. We find no clear relationship between the mobility and the laser power for the untreated sample. However, we obtain a good power law fit to the mobility scaling as $\mu \propto P^{0.64}$ above laser powers of 10^{-3} mW. The dependence of the photocurrent on the laser power is sub-linear, although the power law response is enhanced by plasma treatment from $\mu \propto P^{0.13}$ to $\mu \propto P^{0.29}$ (see Fig. S1).

We plot the DC photoresponsivity, R_{ph} , at different gate biases as a function of irradiation power in Fig. 3. R_{ph} is the current generated in the device per unit of laser power and is a crucial parameter that quantifies the sensitivity of photodetectors.³² We obtain good linear fits of R_{ph} as a function of power, P , across the whole gate bias range, before and after plasma treatment. The negative slope in the log-log plot indicates the saturation of trap states in the material with increasing incident optical power.^{3,5,16} In Fig. 3(a), we see the 0 V and 60 V gate bias trends exhibiting similar levels of R_{ph} , especially at higher laser powers. Upon plasma treatment, in Fig. 3(b), we observe an enhancement of R_{ph} for all tested gate biases and a notable separation of the responsivity as a function of V_g . As V_g is increased, the device becomes more responsive to laser illumination. The slope of this relationship depends on the charge trapping rate in the MoS₂ FET channel.^{29,37} Our results suggest that the presence of plasma-created oxides on the surface inhibits photo-generated pair recombination via defect sites. When compared at $V_g = 60$ V where the FET moves into depletion, i.e., the majority carrier concentration in MoS₂ induced by gating begins to approach that of the photogenerated carrier density,³⁸ the dependence on laser power is stronger for the treated sample. This also serves as a measure of the photogating effect seen in the power-graded transfer curves in Figs. 2(a) and 2(b). An increased response after plasma treatment is thus a direct consequence of the additional charge present in the device, as demonstrated by higher current levels in the gate curves.

The temporal response of the device pre- and post-plasma treatment is charted in Fig. 3(c). The photocurrent is seen to improve two-fold for the tested device when the laser irradiation is modulated through 5 s on/off cycles at a power of $36 \mu\text{W}$ and $V_{ds} = 5$ V. The post-sensitization fall (τ_{fall}) and rise (τ_{rise}) times are extracted from single

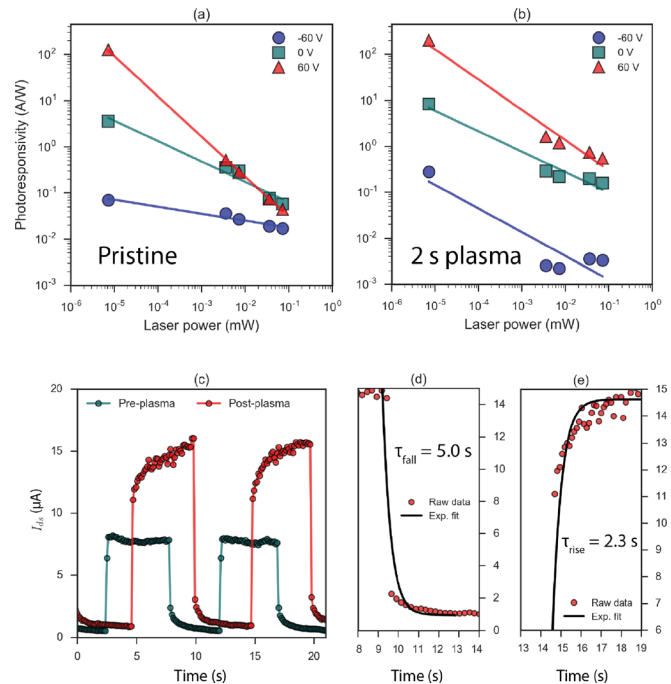


FIG. 3. (a) R_{ph} trends for the untreated MoS₂ sample. (b) Increased responsivity of the MoS₂ phototransistor after 2 s of O₂-Ar plasma treatment. (c) Comparison of the temporal photocurrent response over laser irradiation cycles lasting 5 s. (d) Exponential fit of the fall component of the photoresponse for the treated device. (e) Exponential fit of the rise component from the next cycle.

exponential fits in Figs. 3(d) and 3(e), respectively. The time-resolved photoresponses compare favorably with the evaporated MoO_x over-layer report,¹² where our rise time at a much lower irradiation power is 35% shorter. However, the response time of the photo-FET has been sacrificed to achieve favourable responsivity. This is a well-known issue in sensitized MoS₂ photo-FETs^{39,40} arising from carrier trapping, and needs to be addressed in future research on these devices.

Spectroscopic mapping of the samples allows for a closer inspection of the chemical state of the MoS₂ surface pre- and post-plasma treatment. Figures 4(a) and 4(b) show the spatially resolved Raman maps of the material corresponding to the in-plane vibrational mode at 385 cm^{-1} . We notice a drastic drop in the intensity of the signal at this frequency, indicating a change in the MoS₂ lattice which alters the Raman-active modes in the sample. The flake-averaged spectra are presented in Fig. 4(c), demonstrating the quenching effect of plasma treatment on the monolayer MoS₂ Raman peaks. From the spectral component fits (see Table S1), the monolayer nature of the sample is confirmed with a wavenumber separation of 20.5 cm^{-1} between the A_1' and E' peaks.⁴¹ Upon plasma treatment, the intensity of both Raman modes is severely reduced after 2 s of exposure, while the peak position also shifts and the full-width-at-half-maximum (FWHM) increases. Both the downshift of the E' peak and upshift of the A_1' peak are consistent with reports on molybdenum oxide formation on MoS₂, as is the asymmetric broadening of both peaks.^{23–25} PL maps of the neutral A exciton emission (1.84 eV) of the same flake are presented before and after 2 s of plasma treatment in Figs. 4(d) and 4(e).

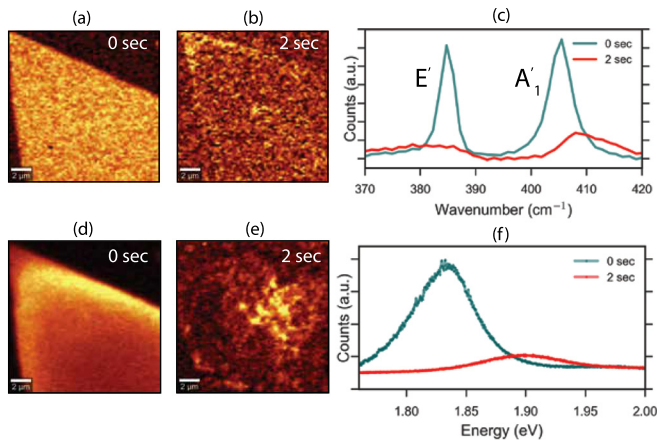


FIG. 4. Raman maps of a monolayer flake before (a) and after (b) plasma treatment, filtered for the in-plane E' mode at 385 cm^{-1} . (c) Raman spectra averaged from the flake area. PL maps of the same flake before (d) and after (e) treatment tracking the direct A exciton emission. (f) Averaged PL spectra from the same flake area.

Accompanying spectra averaged across the whole sample are shown in Fig. 4(f). We observe significant quenching of direct excitonic recombination in the sample after the plasma introduces the oxide species on the surface (see Fig. S3 for TEM images). The emission is also largely blue shifted to higher energies by $\sim 0.1\text{ eV}$. These observations are also in line with previous studies of oxidized MoS_2 , where the monolayer PL emission intensity is reduced and blueshifts due to the presence of sub-stoichiometric oxides on the surface as a function of plasma exposure time.^{25,42}

We suggest that the observed photoresponsivity improvement results from carrier trapping at the lateral $\text{MoS}_2/\text{MoO}_x$ heterojunction interface.¹² The electron affinity and bandgap of monolayer MoS_2 are $\sim 4.3\text{ eV}$ and 1.8 eV , respectively.^{1,43} After the rapid plasma treatment, MoO_x is generated on the device surface as demonstrated in the previous discussion. In Fig. 5(a), we present a SEM image of plasma-treated MoS_2 , where small regions of high work function material (dark contrast) are seen nested on the MoS_2 surface.

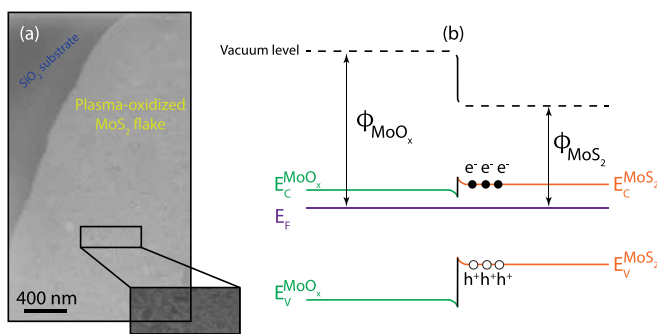


FIG. 5. (a) SEM micrograph of plasma-treated MoS_2 showing dark contrast areas of MoO_x . The inset shows a magnified region with the contrast increased, highlighting the presence of the dark regions. (b) Representative band diagram of the equilibrated $\text{MoS}_2/\text{MoO}_x$ heterojunction, visualising the trapping of photogenerated holes at the interface.

Oxides of molybdenum are commonly known as high work function materials (6.8 eV) with a bandgap of 3 eV ,^{12,42} and hence appear darker in secondary electron micrographs than the lower work function MoS_2 at this electron beam energy (15 keV). Uniformly distributed plasma-generated oxides spanning tens of nanometers form an effective medium with the unreacted MoS_2 in the FET channel, as observed more clearly in the contrast-adjusted inset on the micrograph in Fig. 5(a) (see also scanning transmission electron microscopy results for nanometer-resolved images of pits in our previous work²⁵). As the Fermi level of the donor MoS_2 is higher than that of MoO_x , significant band bending will occur at the equilibrated interface of the heterojunction.⁴⁴ Photo-generated holes in MoS_2 will become trapped at the junction interface,⁴⁵ inhibiting radiative recombination and thereby enhancing the photocurrent with electrons as majority carriers, as previously pointed out by Yoo *et al.*¹² and outlined in the band diagram in Fig. 5(b). This observation is also supported by the suppressed radiative recombination observed in the PL data and the strong photogating effect mediated by the electron-rich FET channel. The improved responsivity at higher back-gate fields is a direct consequence of Fermi level alignment which also facilitates easier photocarrier injection into the contacts^{8,46,47} and primes the device for photon detection levels exceeding those of the pristine MoS_2 .

In that conclusion, we have demonstrated that the photoresponsivity of MoS_2 monolayer FETs can be enhanced ten-fold by the introduction of surface-bound molybdenum oxides. The effect of the mobility and photoresponsivity enhancement depends on laser power and is more prominent at powers exceeding several μWatts .

See [supplementary material](#) for details on the spectroscopic fits, power dependence of current, 4 s exposure data, and TEM images.

REFERENCES

- K. F. Mak, C. Lee, J. Hone, J. Shan, and T. F. Heinz, *Phys. Rev. Lett.* **105**, 136805 (2010).
- H. Qiu, L. Pan, Z. Yao, J. Li, Y. Shi, and X. Wang, *Appl. Phys. Lett.* **100**, 123104 (2012).
- O. Lopez-Sanchez, D. Lembke, M. Kayci, A. Radenovic, and A. Kis, *Nat. Nanotechnol.* **8**, 497 (2013).
- X. Wang, Y. Cui, T. Li, M. Lei, J. Li, and Z. Wei, *Adv. Opt. Mater.* **7**, 1801274 (2019).
- X. Wang, P. Wang, J. Wang, W. Hu, X. Zhou, N. Guo, H. Huang, S. Sun, H. Shen, T. Lin *et al.*, *Adv. Mater.* **27**, 6575 (2015).
- A. E. Yore, K. K. Smithe, S. Jha, K. Ray, E. Pop, and A. Newaz, *Appl. Phys. Lett.* **111**, 043110 (2017).
- H. Wang, C. Zhang, W. Chan, S. Tiwari, and F. Rana, *Nat. Commun.* **6**, 8831 (2015).
- Z. Yin, H. Li, H. Li, L. Jiang, Y. Shi, Y. Sun, G. Lu, Q. Zhang, X. Chen, and H. Zhang, *ACS Nano* **6**, 74 (2012).
- S. Lee, Y. Park, G. Yoo, and J. Heo, *Appl. Phys. Lett.* **111**, 223106 (2017).
- S.-W. Wang, H. Medina, K.-B. Hong, C.-C. Wu, Y. Qu, A. Manikandan, T.-Y. Su, P.-T. Lee, Z.-Q. Huang, Z. Wang *et al.*, *ACS Nano* **11**, 8768 (2017).
- Y. Yang, N. Huo, and J. Li, *J. Mater. Chem. C* **5**, 11614 (2017).
- G. Yoo, S. Hong, J. Heo, and S. Kim, *Appl. Phys. Lett.* **110**, 053112 (2017).
- D. Kufer, I. Nikitskiy, T. Lasanta, G. Navickaite, F. H. Koppens, and G. Konstantatos, *Adv. Mater.* **27**, 176 (2015).
- D. Kufer, T. Lasanta, M. Bernechea, F. H. Koppens, and G. Konstantatos, *ACS Photonics* **3**, 1324 (2016).
- J. J. Gough, N. McEvoy, M. O. Evoy, A. P. Bell, D. McCloskey, J. B. Boland, J. N. Coleman, G. S. Duesberg, and A. L. Bradley, *Adv. Funct. Mater.* **28**, 1706149 (2018).
- S. H. Yu, Y. Lee, S. K. Jang, J. Kang, J. Jeon, C. Lee, J. Y. Lee, H. Kim, E. Hwang, S. Lee, and J. H. Cho, *ACS Nano* **8**, 8285 (2014).

- ¹⁷D.-H. Kang, M.-S. Kim, J. Shim, J. Jeon, H.-Y. Park, W.-S. Jung, H.-Y. Yu, C.-H. Pang, S. Lee, and J.-H. Park, *Adv. Funct. Mater.* **25**, 4219 (2015).
- ¹⁸Y. Huang, W. Zheng, Y. Qiu, and P. Hu, *ACS Appl. Mater. Interfaces* **8**, 23362 (2016).
- ¹⁹J. Miao, W. Hu, Y. Jing, W. Luo, L. Liao, A. Pan, S. Wu, J. Cheng, X. Chen, and W. Lu, *Small* **11**, 2392 (2015).
- ²⁰W. Jing, N. Ding, L. Li, F. Jiang, X. Xiong, N. Liu, T. Zhai, and Y. Gao, *Opt. Express* **25**, 14565 (2017).
- ²¹M. R. Islam, N. Kang, U. Bhanu, H. P. Paudel, M. Erementchouk, L. Tetard, M. N. Leuenberger, and S. I. Khondaker, *Nanoscale* **6**, 10033 (2014).
- ²²F. Giannazzo, G. Fisichella, G. Greco, S. Di Franco, I. Deretzis, A. La Magna, C. Bongiorno, G. Nicotra, C. Spinella, M. Scopelliti *et al.*, *ACS Appl. Mater. Interfaces* **9**, 23164 (2017).
- ²³T. Y. Ko, A. Jeong, W. Kim, J. Lee, Y. Kim, J. E. Lee, G. H. Ryu, K. Park, D. Kim, Z. Lee *et al.*, *2D Mater.* **4**, 014003 (2016).
- ²⁴N. Choudhary, M. R. Islam, N. Kang, L. Tetard, Y. Jung, and S. I. Khondaker, *J. Phys.: Condens. Matter* **28**, 364002 (2016).
- ²⁵J. Jadwiszczak, C. O'Callaghan, Y. Zhou, D. S. Fox, E. Weitz, D. Keane, C. P. Cullen, I. O'Reilly, C. Downing, A. Shmeliov *et al.*, *Sci. Adv.* **4**, eaao5031 (2018).
- ²⁶J. Jadwiszczak, Y. Zhou, and H. Zhang, *MRS Commun.* **8**, 514 (2018).
- ²⁷S. I. Khondaker and M. R. Islam, *J. Phys. Chem. C* **120**, 13801 (2016).
- ²⁸M. O'Brien, N. McEvoy, T. Hallam, H.-Y. Kim, N. C. Berner, D. Hanlon, K. Lee, J. N. Coleman, and G. S. Duesberg, *Sci. Rep.* **4**, 7374 (2014).
- ²⁹W. Zhang, J.-K. Huang, C.-H. Chen, Y.-H. Chang, Y.-J. Cheng, and L.-J. Li, *Adv. Mater.* **25**, 3456 (2013).
- ³⁰W. Tang, C. Liu, L. Wang, X. Chen, M. Luo, W. Guo, S.-W. Wang, and W. Lu, *Appl. Phys. Lett.* **111**, 153502 (2017).
- ³¹M. J. Park, K. Park, and H. Ko, *Appl. Surf. Sci.* **448**, 64 (2018).
- ³²C. Xie, C. Mak, X. Tao, and F. Yan, *Adv. Funct. Mater.* **27**, 1603886 (2017).
- ³³C. Garcia, N. Pradhan, D. Rhodes, L. Balicas, and S. McGill, *J. Appl. Phys.* **124**, 204306 (2018).
- ³⁴J. Guo, B. Yang, Z. Zheng, and J. Jiang, *Phys. E* **87**, 150 (2017).
- ³⁵S. Chuang, C. Battaglia, A. Azcatl, S. McDonnell, J. S. Kang, X. Yin, M. Tosun, R. Kapadia, H. Fang, R. M. Wallace *et al.*, *Nano Lett.* **14**, 1337 (2014).
- ³⁶S. McDonnell, A. Azcatl, R. Addou, C. Gong, C. Battaglia, S. Chuang, K. Cho, A. Javey, and R. M. Wallace, *ACS Nano* **8**, 6265 (2014).
- ³⁷M. Massicotte, P. Schmidt, F. Violla, K. G. Schaedler, A. Reserbat-Plantey, K. Watanabe, T. Taniguchi, K.-J. Tielrooij, and F. H. Koppens, *Nat. Nanotechnol.* **11**, 42 (2016).
- ³⁸C.-C. Wu, D. Jariwala, V. K. Sangwan, T. J. Marks, M. C. Hersam, and L. J. Lauhon, *J. Phys. Chem. Lett.* **4**, 2508 (2013).
- ³⁹D.-H. Kang, S. R. Pae, J. Shim, G. Yoo, J. Jeon, J. W. Leem, J. S. Yu, S. Lee, B. Shin, and J.-H. Park, *Adv. Mater.* **28**, 7799 (2016).
- ⁴⁰J. He, Y. Yang, Y. He, C. Ge, Y. Zhao, L. Gao, and J. Tang, *ACS Photonics* **5**, 1877 (2018).
- ⁴¹H. Li, Q. Zhang, C. C. R. Yap, B. K. Tay, T. H. T. Edwin, A. Olivier, and D. Baillargeat, *Adv. Funct. Mater.* **22**, 1385 (2012).
- ⁴²N. Kang, H. P. Paudel, M. N. Leuenberger, L. Tetard, and S. I. Khondaker, *J. Phys. Chem. C* **118**, 21258 (2014).
- ⁴³Y. Liang, S. Huang, R. Soklaski, and L. Yang, *Appl. Phys. Lett.* **103**, 042106 (2013).
- ⁴⁴Z. Zhang and J. T. Yates, Jr., *Chem. Rev.* **112**, 5520 (2012).
- ⁴⁵M. M. Furchi, D. K. Polyushkin, A. Pospischil, and T. Mueller, *Nano Lett.* **14**, 6165 (2014).
- ⁴⁶D. Kufer and G. Konstantatos, *Nano Lett.* **15**, 7307 (2015).
- ⁴⁷C. Chen, H. Qiao, S. Lin, C. Man Luk, Y. Liu, Z. Xu, J. Song, Y. Xue, D. Li, J. Yuan *et al.*, *Sci. Rep.* **5**, 11830 (2015).